JACS
JOURNAL OF THE AMERICAN CHEMICAL SOCIETY

Article

pubs.acs.org/JACS

How Ag Nanospheres Are Transformed into AgAu Nanocages

Liane M. Moreau,[†,⊥] Charles A. Schurman,[‡,⊥] Sumit Kewalramani,[†,⊥] Mohammad M. Shahjamali,[§,⊥] Chad A. Mirkin,*[,†,‡,§,⊥] and Michael J. Bedzyk*[,†,∥,⊥]

[†]Department of Materials Science and Engineering, [‡]Department of Biomedical Engineering, [§]Department of Chemistry, [∥]Department of Physics and Astronomy, and [⊥]International Institute for Nanotechnology, Northwestern University, Evanston, Illinois 60208, United States

Supporting Information

ABSTRACT: Bimetallic hollow, porous noble metal nanoparticles are of broad interest for biomedical, optical and catalytic applications. The most straightforward method for preparing such structures involves the reaction between $HAuCl_4$ and well-formed Ag particles, typically spheres, cubes, or triangular prisms, yet the mechanism underlying their formation is poorly understood at the atomic scale. By combining in situ nanoscopic and atomic-scale characterization techniques (XAFS, SAXS, XRF, and electron microscopy) to follow the process, we elucidate a plausible reaction pathway for the conversion of citrate-capped Ag nanospheres to AgAu nanocages; importantly, the hollowing event cannot be explained by the nanoscale Kirkendall effect, nor by Galvanic exchange alone, two processes that have been previously proposed. We propose a modification of the bulk Galvanic exchange process that takes into account considerations that can only occur with nanoscale particles. This *nanoscale* Galvanic exchange process explains the novel morphological and chemical changes associated with the typically observed hollowing process.

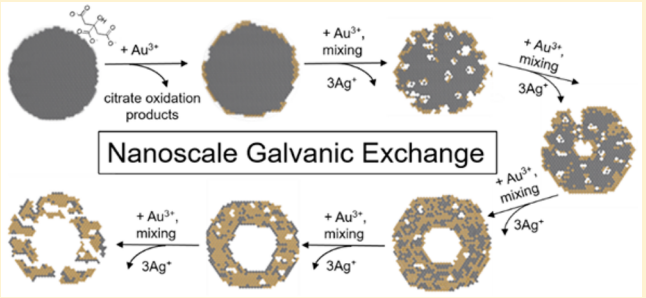

INTRODUCTION

Noble metal nanoparticles are of great interest due to their unusual properties that differ from their bulk counterparts.[1−3] Hollow nanoparticles are of particular interest due to their ability to encapsulate molecular moieties,[4,5] as well as the unique optical properties that emerge from their geometry.[6−8] Bimetallic particles are interesting for their catalytic[9−11] and optical properties.[12] Bimetallic AuAg nanocages synthesized from Ag sacrificial templates through titration with an Au^{3+} salt[13−16] are widely used in photothermal medical applications[8,17−20] and catalysis,[21−24] as well as in metallic corrosion studies.[25] This general reaction has been used to prepare a wide variety of hollow particles regardless of geometry.[13,26−32] In addition, variants of this redox process have been used to prepare bimetallic particles consisting of AgPt,[33,34] AgPd,[34] AuCu,[35] CuPd,[36] CuPt,[36,37] PdPt,[10] CoAu,[38] and PtCo.[39] Despite this versatility and utility, the mechanism underlying these reactions remain elusive.

The reaction converting Ag nanoparticles to Au nanocages is commonly referred to as "Galvanic exchange":

$$3Ag_{(s)} + AuCl_{4(aq)}^{-} \rightarrow Au_{(s)} + 3Ag_{(aq)}^{+} + 4Cl_{(aq)}^{-} \quad (1)$$

Specifically, at a surface, the reaction proceeds because the standard reduction potential of the $AuCl_4^-$/Au redox pair (0.99 V vs the standard hydrogen electrode (SHE)) is higher than that of the Ag+/Ag redox pair (0.80 V vs SHE) (Figure 1, top). The template material becomes a uniformly porous network as Ag atoms are removed from the template in a 3:1 Ag:Au ratio and vacancies coalesce to reduce surface energy. Due to differences in Ag−Ag, Ag−Au and Au−Au bond energies, the created alloy exhibits local phase segregation with Ag and Au-rich regions.[40] While some have attributed the nanoparticle hollowing to the above-described bulk Galvanic exchange effect,[14,41−44] others have attributed the hollowing process to the Kirkendall effect (Figure 1 bottom).[26,29,31,45−48] In the Kirkendall effect, voids are formed due to a difference in the diffusion rate of the core atoms outward, which exceeds the rate of the added secondary species inward into the nanoparticle core.[48,49] For the case of AgAu nanoparticle formation, according to this explanation, Ag diffuses more quickly into Au than Au into Ag resulting in a uniform, homogeneous AgAu shell surrounding a hollow core. In this process, no Ag is lost from the nanoparticle with Au addition, resulting in an overall increase in the number of atoms present in the nanoparticle, as seen for other model systems exhibiting the nanoscale Kirkendall effect.[50−52] Our present study aims to resolve this controversy and elucidate the reaction pathway with atomistic detail.

We explore the conversion from citrate-capped Ag nanospheres to AgAu nanocages and find that the hollowing within the nanoparticles cannot be explained by the nanoscale Kirkendall effect nor Galvanic exchange alone. This conclusion is reached through in-depth nano and atomic scale characterization of the nanoparticles at various stages in their

Received: June 28, 2017
Published: August 11, 2017

DOI: 10.1021/jacs.7b06724
J. Am. Chem. Soc. 2017, 139, 12291−12298

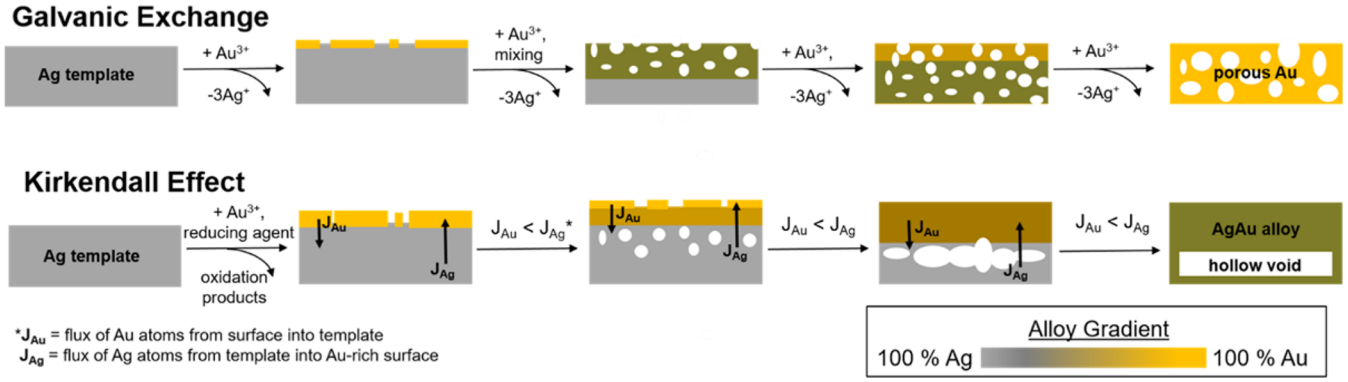

Figure 1. Galvanic exchange and Kirkendall effect. Two hypothesized bulk processes used to explain the formation of AgAu nanocages from Ag nanoparticle templates include Galvanic exchange (top) and the Kirkendall effect (bottom).

transformation. Overall, we propose a modification of the bulk Galvanic exchange process that takes into account considerations that can only occur with nanoscale particles. We refer to this modified process as "nanoscale Galvanic exchange".

Before going further, it is important to consider previous studies that provide insight into this particular nanoparticle transformation at the nanoscale. Electron microscopy studies[1,8,41,42,53] revealed formation of a hollow, porous product and minimal growth of the template particle attributed to an initial Au surface monolayer formation. Pit formation at the surface provides an active site for Ag oxidation. With additional $HAuCl_4$ incorporation, UV−vis spectroscopy revealed a shift to longer wavelengths in the localized surface plasmon resonance (LSPR) peak throughout the visible regime and into the near-IR,[1,8] which is expected for a change in morphology toward a hollowed-out structure.[45] The aforementioned features observed are in line with what would be expected for Galvanic exchange, however void formation is observed, which is a structural feature associated with the Kirkendall effect,[50−52] and not with bulk Galvanic exchange, where a uniformly porous network is formed.[40,54] Electron tomography of single nanoparticles was used to track 3D void and pit formation.[55] Reaction kinetics of void formation were investigated using dark-field scattering,[56] and indicated an abrupt transition into a hollow nanocage structure. Supporting theoretical work[56] concluded that this abrupt transition was due to the energetic favorability of vacancy coalescence into a central void to minimize particle surface area. This provides an alternative explanation for the nanoparticle hollowing process based on nanoscale geometry.

In each of the aforementioned studies, the transformation from Ag nanoparticles to AgAu nanocages was referred to as "Galvanic exchange", yet there is no atomic-scale information used to inform this conclusion. To this end, we formulate a series of questions that will serve as a foundation for elucidating the chemical pathway and will be addressed in detail through a combination of literature findings and new experimental results: (1) How does the 3D morphology of the nanoparticles evolve as the reaction progresses? (2) How is the nanoparticle reaction initiated? (3) Does the total number of atoms within the nanoparticle increase or decrease? Is there a 3:1 Ag:Au exchange ratio? (4) Is a homogeneous alloy or is local segregation observed? (5) What is the origin of the nanoparticle hollowing process?

Questions 1 and 2 pertain to nanoparticle structure on the nanometer length scale. In part, these questions have already been answered through use of electron microscopy and tomography.[1,8,41,42,53,55] Yet due to a lack of previous atomic-scale characterization, questions 3−5 remain unaddressed. Our experimental contribution to this work fills in this gap in atomic-scale characterization by use of Å-wavelength X-rays. Specifically, we use X-ray absorption fine structure (XAFS) to locally track the atomistic changes as a function of reaction progression. These changes are then correlated with changes in the globally averaged morphological parameters derived from small-angle X-ray scattering (SAXS) measurements.

To rule out surface-facet effects on the transformation process as hypothesized elsewhere,[28,42] citrate-capped polycrystalline Ag nanospheres[57] were chosen as the starting nanoparticle template. These have been previously used to make AgAu nanocages and the reaction has been reported to proceed via Galvanic replacement.[56,58−60] $HAuCl_4$ was titrated in varying amounts to an aqueous solution of Ag nanosphere templates and the resulting transformed nanoparticles were studied as a function of reaction stage (Figure 2). Through characterization with conventional electron microscopy and UV−vis spectroscopy in combination with XAFS, X-ray fluorescence (XRF) and SAXS, local and global atomic and nanoscale trends can be explored in depth, as evidenced by previous studies of Ag and Au alloy nanoparticles using an X-

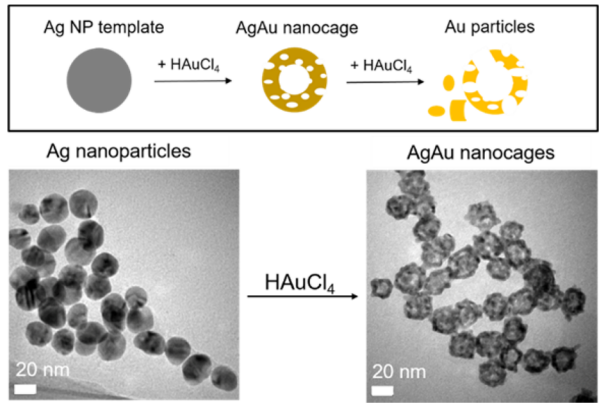

Figure 2. Synthesis transformation reaction schematic. Polycrystalline citrate-capped Ag nanoparticles (scale bar = 20 nm) starting at room temperature (left) are transformed into AgAu nanocages of a hollow and porous nature (right, 62.9 at% Au) with increasing addition of 0.1 mM $HAuCl_4$. A cartoon representation of the synthesis products are shown (top). As additional $HAuCl_4$ is added, the particles lose their structural integrity.

DOI: 10.1021/jacs.7b06724
J. Am. Chem. Soc. 2017, 139, 12291−12298

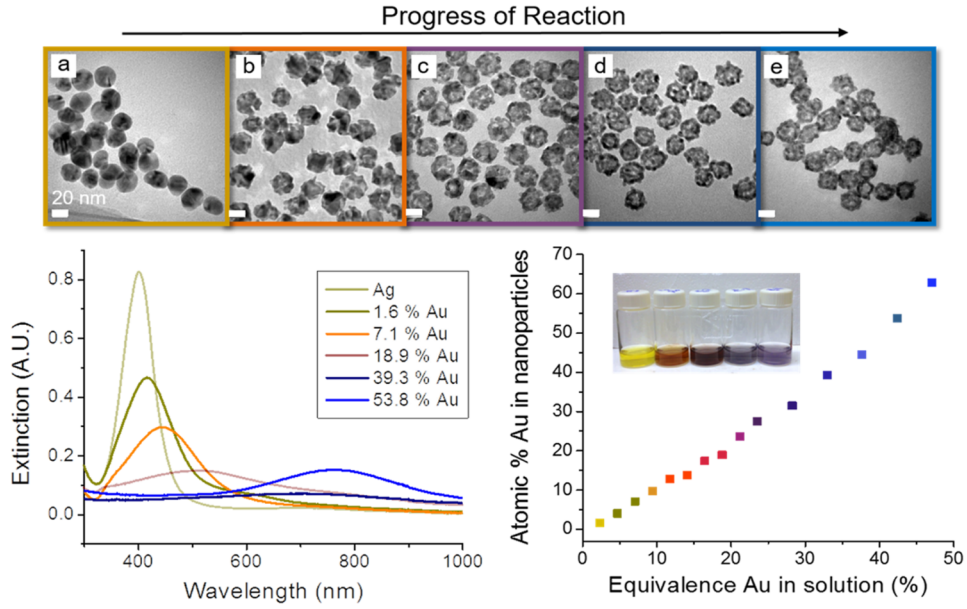

Figure 3. Nanoparticle products as a function of $HAuCl_4$ addition. (Top) TEM images from pure citrate-capped Ag NPs (a) to (b) 4.0%, (c) 9.8%, (d) 27.5% and (e) 62.9% Au as determined by XRF. All scale bars are 20 nm. (Bottom, left) UV−vis spectra reveal LSPR peak shifts to longer wavelengths with additional $HAuCl_4$ (right, inset). (Bottom, right) Atomic % Au in the nanoparticles as determined by XRF vs equivalence Au added into the reaction solution.

ray focused approach.[61−64] Thus, our characterization toolbox provides us with structural insight into the previously posed questions and enables us to propose a plausible reaction pathway for the transformation from citrate-capped Ag nanospheres to AgAu nanocages.

METHODS

For each of the methods described below, more details can be found in the Supporting Information (SI).

Synthesis. Transformation of Ag nanoparticles into hollow AgAu nanocages was performed using a variation on previous methods.[65] $HAuCl_4$ (Sigma-Aldrich) was dissolved in NANOpure water (18.2 MΩ ionic purity) to a concentration of 0.1 mM in solution. This solution (the source of Au^{3+} ions) was then titrated into a vial of 3 pM 18 nm diameter citrate capped silver spheres in aqueous 2 mM sodium citrate solution (Ted Pella) using a syringe pump at a rate of 20 mL/h at room temperature. $HAuCl_4$ solution was added in different amounts to equal volumes of Ag particles in order to halt the reaction at different stages of transformation. Transformed particles were then isolated through high-speed centrifugation.

UV−Vis Spectroscopy. UV−vis spectroscopy scans of samples in 1 mL of NANOpure water were taken using a Cary 5000 UV−vis spectrophotometer across the range of 200−1000 nm at a 1 cm path length.

Inductively Coupled Plasma−Mass Spectroscopy (ICP-MS). Au content in the nanoparticles and supernatant was analyzed using a Thermo Fisher X Series II ICP-MS system at the QBIC Facility at Northwestern University (NU). Particles were dissolved in aqua regia for 24 h before measurement. Au content in ppb was determined through comparison against a standard curve generated using Au ICP standard (Sigma-Aldrich). An internal In standard was also used.

Electron Microscopy. Using the NU EPIC Facility, samples were prepared for characterization with electron microscopy by dropcasting on a carbon-coated grid. TEM images were collected using a Hitachi H-8100 TEM at 200 keV. STEM images and EDX maps were collected using a Hitachi HD-2300 Dual EDS S/TEM at 200 keV. Drift correction was used for EDX mapping in order to improve spatial resolution.

X-ray Scattering. Small angle X-ray scattering (SAXS) measurements were performed using 10.00 keV X-rays at SID-D located at the Advanced Photon Source (APS) at the Argonne National Laboratory (ANL). This is part of the NU operated DND-CAT Facility. The aqueous nanoparticle dispersions were placed in a quartz capillary tube (inner diameter ~1.5 mm), which was embedded in a flow cell.

The measured intensity profile $I(q)$ is reasonably described by assuming a spherical core−shell model for the form factor $[F(q)]$ of the Ag and Ag/Au bimetallic nanoparticles.[66] Specifically,

$$F(q) = \frac{4\pi}{q^3}[(\rho_c - \rho_s)\{\sin[qR_c] - qR_c\cos[qR_c]\} + (\rho_s - \rho_{sol})\{\sin[q(R_c + T_s)] - q(R_c + T_s)\cos[q(R_c + T_s)]\}] \quad (2)$$

Here, R_c is the radius of the hollowed-out core for the Ag/Au alloy nanoparticles. For unalloyed pure Ag nanoparticles, $R_c = 0$. The electron density ρ_c for the hollowed-out core is assumed equivalent to the water solvent ($\rho_c = \rho_{sol} = 334\ e^-/nm^3$). T_s is the radial thickness of the metallic shell, ρ_s is the electron density for the shell, and

$$I(q) = \frac{N}{V} r_e^2 \langle [F(q)]^2 \rangle + bkg \quad (3)$$

To take into account the polydispersity (PD) of nanoparticles, the scattered intensity from an isolated nanoparticle $[F(q)]^2$ is averaged over a Schulz distribution[67] for particle sizes to yield $\langle [F(q)]^2 \rangle$ Here, the ratio of core radius and the shell thickness $[R_c/T_s]$ is assumed to be a constant for all the AgAu particles in a given solution. r_e is the classical electron radius and N/V is the number density of nanoparticles in the solution. The constant *bkg* represents any additional background scattering apart from the quartz capillary and water.

XAFS. XAFS spectra at the Au L_3 edge and Ag K edge (11.919 and 25.514 keV, respectively) were collected at MR-CAT station 10BM-B located at the APS. Energy scans were taken over a range from −150 to 600 eV with respect to the Au or Ag absorption edge using a Si(111) monochromator. XAFS spectra were collected in X-ray fluorescence (XRF) mode using a four-element Vortex Silicon drift-diode (SDD) detector, calibrated with an Au or Ag metal foil standard. Samples were concentrated via centrifugation to micromolar concentrations of Au/Ag atoms and placed in 3 mm inner diameter quartz capillary tubes.

DOI: 10.1021/jacs.7b06724
J. Am. Chem. Soc. 2017, 139, 12291−12298

XAFS data was processed using ATHENA and ARTEMIS software, part of the IFEFFIT package.[68] The extended XAFS (EXAFS) regions of the spectra were modeled according to the EXAFS equation:[69−72]

$$\chi(k) = \sum_{\Gamma}\left[\frac{N_\Gamma S_0^2 F_\Gamma(k)}{2kR_\Gamma^2} e^{-2k^2\sigma_\Gamma^2} e^{-2R_\Gamma/\lambda(k)} \times \sin(2kR_\Gamma + \phi_\Gamma(k))\right] \quad (4)$$

where Γ is the summation over the individual scattering pathways included in the model, k is the photoelectron wavevector, $F_\Gamma(k)$ is the scattering amplitude, $\lambda(k)$ is the mean free path of inelastically scattered photoelectrons and $\Phi(k)$ is the phase shift, which is calculated as a function of the absorbing and scattering atom. S_0^2, the amplitude reduction factor, was set to the value extracted from fitting a bulk Au or Ag foil as applicable. This enables a more accurate determination of the coordination number.[71] Degeneracy (N_Γ), interatomic distance (R_Γ), energy shift parameter (E_0), and mean-squared disorder ($\sigma_\Gamma 2$), which includes contributions from structural and thermal disorder (Debye−Waller factor),[69] were adjusted to determine the best fit model.

XRF Methods. X-ray fluorescence spectra (Figure S3) were obtained at APS sector 10BM-B using a Vortex four element silicon drift diode detector. Spectra were collected at 26.014 keV (above the Ag K edge energy, 25.514 keV) to determine the Ag-to-Au atomic ratio from the areas under the Au L alpha and Ag K alpha fluorescence lines, with fluorescence peak fits using a Gaussian function. Elemental XRF cross sections, detector efficiency, and attenuation due to solvent media were taken into account in determining the Ag/Au ratio.

RESULTS

1. How Does the 3D Morphology of the Nanoparticles Evolve as the Reaction Progresses? TEM and UV−vis spectroscopy confirm previously observed morphological trends, showing that results from our study are relevant to prior work.[1,8,41,42,53] These morphological changes are correlated to the amount of Au incorporation (in atomic %) into the NPs determined by XRF (Figure 3, bottom-right).

TEM (Figure 3, top) shows that the initial quasi-spherical Ag nanoparticles are ∼20 nm in diameter. Pits form at the nanoparticle surface and a hollow center appears. As additional $HAuCl_4$ is added, the interior void in the nanoparticle grows as the shell porosity increases, resulting in hollow and porous nanocages with 62.9% Au incorporation. As observed previously, above ∼65% Au, the particles lose their structural integrity and deteriorate into small, irregular particles.[42,73] UV−vis spectroscopy (Figure 3, bottom-left) shows that the LSPR peak red-shifts as a function of $HAuCl_4$ addition. This allows for tunable optical properties throughout the visible regime.

SAXS data and model fits based on eq 2 are shown in Figure S6. This analysis enables tracing 3D hollow void formation and shell thickness evolution in a globally statistical manner that is summarized in Figure 4. We observe that the hollow core radius increases in size until ∼25% Au, while the shell thickness decreases. Above 25% Au, we find that these geometrical parameters remain relatively constant, while the porosity of the shell (based on TEM, Figure 3, top) continues to increase. Thus, after a critical void size is reached, particle transformation with continued $HAuCl_4$ addition occurs only at the atomic scale. SAXS and local (TEM) analysis of nanoparticle size (Figure S10) both show that within error, the nanoparticles do not change their overall size from the original template structure. This observation is inconsistent with a hollowing process based on the Kirkendall effect, where an increase in size would be expected[50−52] Figure 1.

2. How Is the Nanoparticle Reaction Initiated? TEM images early in the reaction (Figure 3, top) show apparent pits

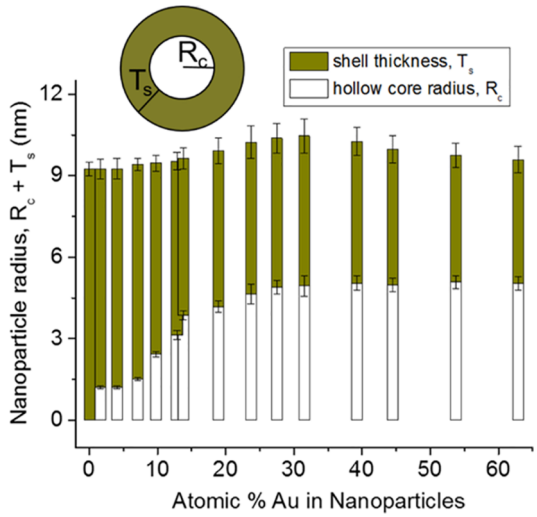

Figure 4. Nanoparticle morphological trends from SAXS modeling, which determines the ensemble averaged inner and outer radii of the hollowed-out NPs. With increasing Au incorporation, the shell thickness (gold) decreases, while the radius of the core (white) increases, as additional Ag atoms are removed from the core. The overall radius of the particle does not significantly change.

and a nonuniform structure at the nanoparticle surface. This suggests that transformation has occurred at the nanoparticle surface before voids and porosity are observed in the interior. It has previously been suggested that Au(0) coats the nanoparticle surface before transformation occurs.[41,42] Our ICP and XRF data at the initial 1.6% Au shows a Ag:Au replacement ratio (Table S1) that is less than unity (0.5 ± 0.1), indicating the addition of 2 Au atoms onto the nanoparticle surface for every Ag atom removed. This means that more Au atoms are added than Ag atoms replaced. If the Au was depositing onto the surface at this initial stage, then the 1.6% Au and SAXS-determined 18 nm diameter NP would correspond to 0.8 monolayers of Au incorporated in the NP surface atomic layer, assuming bulk-like atomic densities. This observation suggests that at this stage, Ag cannot be the sole reducing agent.

3. Does the Total Number of Atoms within the Nanoparticle Increase or Decrease? Is There a 3:1 Ag:Au Exchange Ratio? Nanoparticle hollowing and increasing porosity suggest that the total number of atoms within the nanoparticles decreases with increasing $HAuCl_4$ addition and this is confirmed through calculation of the Ag:Au exchange ratio (Table S1). While after initial Au monolayer deposition the ratio increases to exceed 1:1, meaning an overall loss in the number of atoms within the nanoparticle, the average exchange ratio is significantly less than 3:1. Specifically, at its maximum with 7% Au incorporation, the exchange ratio reaches the expected 3:1, but decreases quickly and is closer to 2:1 until reaction completion. This also is consistent with the conclusion that more than one reducing agent must be involved in the process, and Galvanic replacement cannot exclusively be used to describe this process.

4. Is a Homogeneous Alloy or Local Segregation Observed? EXAFS analysis reveals differences in the phase shifts and scattering amplitudes of the backscattered photoelectrons from Ag and Au atoms as a function of wavevector k, which enables extraction of Ag−Au and Ag−Ag as well as Au−Ag and Au−Au local structure (see Figure S14). EXAFS is a bulk rather than a surface technique, and quantities extracted

DOI: 10.1021/jacs.7b06724
J. Am. Chem. Soc. 2017, 139, 12291−12298

from analysis are representative of the global average particle structure. As expected, the Au−Au and Ag−Au coordination increase while Ag−Ag and Au−Ag decrease with increasing Au incorporation (Figure 5). Yet if we compare the coordination

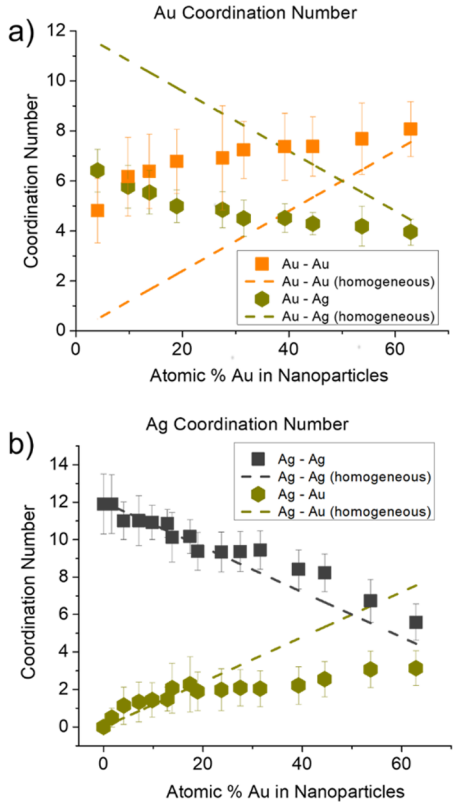

Figure 5. Nanoparticle coordination number trends from EXAFS modeling. (a) Coordination numbers determined from Au L3 edge XAFS. (b) Coordination numbers determined from Ag K edge XAFS. Dashed lines represent the theoretical coordination numbers that would be expected from a homogeneous alloy structure.

numbers with those theoretically expected for a homogeneous alloy, (Figure 5 dashed lines), we find that there is significant deviation. In particular, in a particle that is 62.9% Au, the Ag−Ag coordination exceeds Ag−Au. This observation is confirmed in a model-independent manner by observing that Ag K edge XAFS spectra from nanoparticles with 62.9% Au more closely resembles the spectrum from pure Ag nanoparticles than that from Ag surrounded by Au (Figure 6a). This suggests that rather than forming a homogeneous alloy, Ag-rich and Au-rich clusters of atoms are retained throughout the transformation. Such local segregation is expected for bulk systems[40] and has previously been observed in single-particle electron tomography studies of anisotropic nanocages.[55] The size of these clusters was estimated from the amount of reduction in EXAFS coordination numbers compared to bulk,[74] and found to be slightly below 1 nm in the AgAu nanocages (Figure S5). The nanoscale nature of this phase segregation was investigated using EDX mapping (Figure S4). We find that within the resolution of EDX (~2 nm), Ag and Au are not segregated on this longer length scale. This agrees with EXAFS results and reveals that while the particles are alloyed at the nanoscale, they are compositionally segregated on the atomic scale.

Coordination numbers extracted from EXAFS also provide insight into the nanoparticle surface structure. Figure 6b shows

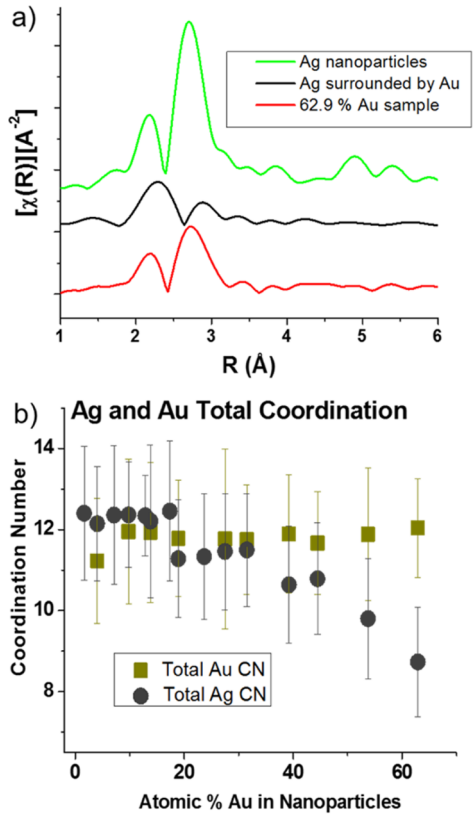

Figure 6. EXAFS informs Ag distribution in AgAu NPs. (a) Ag K-edge Fourier inverted XAFS data for the starting Ag NPs, transformed NPs with 62.9% Au, and a reference sample of Au NPs with trace Ag. (b) From Ag K and Au L3 edge EXAFS, the total Ag and Au coordination numbers within the particles as a function of transformation.

that above 4% Au, the overall Au coordination number remains at ~12, as would be expected for fully coordinated atoms, the coordination number for Ag decreases with increasing nanoparticle porosity throughout the transformation. This suggests that spatially, more Ag rather than Au atoms sit in undercoordinated surface sites, even in Au-rich particles.

5. What Is Origin of the Nanoparticle Hollowing Process? Previous EXAFS studies of the nanoscale Kirkendall hollowing process, which occurs in oxide and phosphide nanoparticles,[50,51] revealed formation of an initial phase in nanoparticle surface layers, after which the diffusion rates of species changed. This leads to faster out-diffusion of the template element than inward diffusion of the secondary element, resulting in nanoparticle hollowing and formation of a new phase, with an entirely different local environment. In our present study, however, the results are not in line with the Kirkendall-system structural changes.

EXAFS local structural changes show a consistent trend; Ag−Au and Au−Au coordination numbers increase linearly while Ag−Ag and Au−Ag coordination numbers decrease linearly (Figure 5). There is no abrupt change in local structure observed. In addition, Kirkendall hollowing induces an increase in the overall particle size, whereas this is not observed by either TEM or SAXS for our system (Figure S10). Rather, our results are in agreement with a previous study which proposed coalescence of vacancies into a critical void in order to reduce the overall surface area in the nanoparticles.[56] TEM images from particles early in the transformation (Figure 3, top) show that either particles exhibit a void or they do not. The void size

DOI: 10.1021/jacs.7b06724
J. Am. Chem. Soc. 2017, 139, 12291−12298

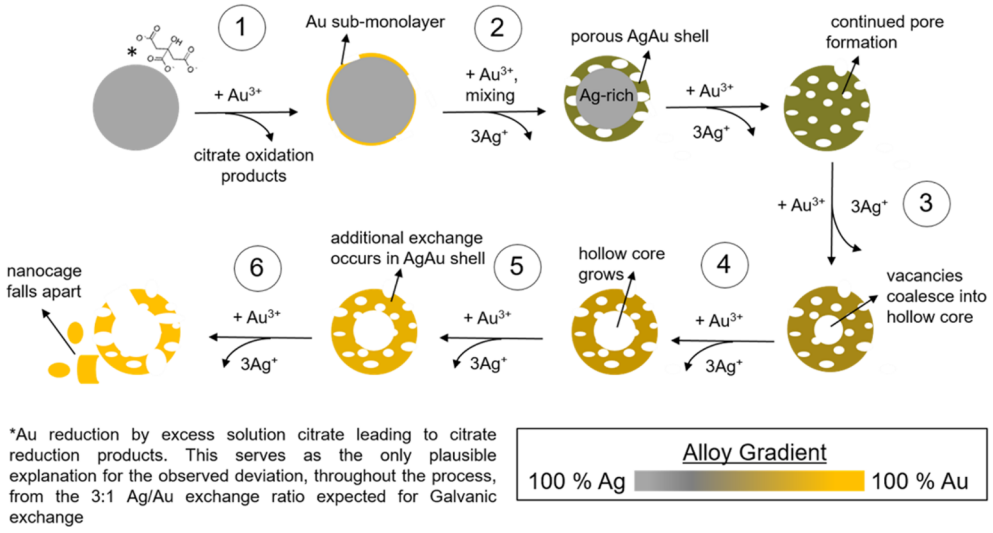

Figure 7. Schematic of the proposed nanoscale Galvanic exchange pathway. Starting with Ag nanospheres (top-left), the nanoparticles transform into AgAu nanocages (bottom-left). Alloy composition is shown in a gradient from Ag (gray) to Au (goldenrod). The included numbers reflect the steps in the process outlined in the text.

observed in these particles from SAXS (2 nm, Figure 4) is also in good agreement with the critical void size observed from the earlier dark-field scattering study.[56] All of this supports the vacancy-coalescence hollowing pathway previously proposed.[56]

DISCUSSION

Comparison to Galvanic Exchange and the Nanoscale Kirkendall Effect. Our results confirm many of the characteristic structural changes that would be expected for the case of Galvanic exchange. For example, TEM confirms a porous product, with local Ag and Au segregation (XAFS). In addition, TEM and SAXS results show that the size of the particles remains nearly constant throughout the entire process. However, there are two key deviations from bulk Galvanic exchange: (1) nanoparticle core hollowing is observed rather than the uniformly porous network that is observed for a bulk film,[40] and (2) while the absolute number of atoms within the nanoparticle does indeed decrease, the Ag:Au exchange ratio deviates substantially from the expected 3:1 ratio.

On the other hand, we do not observe changes in the nanoparticle structure, one would associate with the nanoscale Kirkendall effect. Notably, based on SAXS and TEM analysis, particle size remains nearly constant, and XRF confirms a decrease rather than an increase in the total number of atoms incorporated into the nanoparticle. Our results therefore suggest that the observed hollowing is not the result of the nanoscale Kirkendall effect.

A Modified Pathway: Nanoscale Galvanic Exchange. In order to propose a reaction pathway, we consider deviations the system exhibits from bulk Galvanic exchange. First, nanoparticle hollowing must be accounted for. In bulk films, it is observed that vacancies coalesce to form pores, resulting in a uniformly porous network rather than one larger void.[40] The SAXS results agree with those from a previous study that observe vacancy coalescence into a critical void and describe this process in detail.[56] This, in combination with the lack of structural features expected for Kirkendall hollowing, provides support for the vacancy coalescence hypothesis.[56] Coalescence of vacancies into a hollow void reduces overall surface area in particles for enhanced stability. This variation only occurs on the nanoscale, where particles contain a high surface area to volume ratio.

Second, one must explain why the exchange ratio of Ag:Au is significantly less than 3:1 that defines Galvanic exchange. This implies an additional Au reducing agent rather than Ag etchant must be contributing; as the etchant would cause the ratio to exceed 3:1. Sodium citrate is known to act as a reducing agent for Au^{3+},[75,76] and in this case serves as the only reasonable electron source for Au^{3+} reduction other than Galvanic exchange.[77]

The concentration of citrate present in the reaction solution (2 mM) provides excess electrons (1.2×10^{19}) compared with the number needed to reduce all Au^{3+} added to solution for the 62.9% Au sample (5.6×10^{15}), making this plausible simply from an electron counting standpoint. In addition, the high surface energies due to a high number of coordinatively unsaturated surface atoms, lowers the potential for Au reduction on the nanoparticle surface.

Au deposition onto surface sites along with Galvanic exchange, with both Ag and citrate acting as reducing agents, explains why the exchange ratio of Ag:Au is less than the expected 3:1 ratio if it was purely galvanic exchange. It should be noted that in systems where an alternative particle stabilizing agent (other than citrate) is used or an external reducing agent is introduced, the exchange ratio may differ from those reported here. In fact, it has been previously demonstrated that Au can be deposited on Ag by overcoming the Galvanic exchange pathway through the use of a strong reducing agent such as ascorbic acid[78,79] or by purposefully controlling reaction kinetics even in the case of citrate capped Ag nanoparticles.[76] It should also be noted that anisotropic particles may also induce deviations from the reaction pathway observed in this study due to the introduction of surface-facet specific processes previously proposed.[28,42] Nevertheless, our study provides unique insights into the transformation of citrate-capped Ag nanospheres into AgAu nanocages, as summarized below.

Through the characterization of the system at both the nanometer and atomic length scales, a plausible reaction pathway can be proposed. Since deviations from bulk Galvanic exchange can be explained as a result of the nanoparticle

DOI: 10.1021/jacs.7b06724
J. Am. Chem. Soc. 2017, 139, 12291−12298

synthetic environment and high surface area to volume ratio, we propose that the transformation from Ag nanoparticles to Au nanocages proceeds via nanoscale Galvanic exchange (Figure 7). The process occurs via six key steps. First, $HAuCl_4$ addition to the polycrystalline Ag nanospheres results in deposition of an Au surface monolayer via citrate reduction of the Au^{3+} on the catalytic Ag particle surface. Second, as additional $HAuCl_4$ is introduced into solution, Galvanic exchange between Ag and Au occurs, resulting in Ag replacement with Au, with concomitant Au deposition via citrate reduction, since in the case of citrate-capped Ag particles, citrate acts as an additional source of Ag reduction. Extraction of more Ag than replacement by Au results in vacancy formation in the particle interior as Ag atoms are removed. Third, at a critical concentration of vacancies formed from unequal atomic replacement, spontaneous central void formation from coalesced vacancies in the nanoparticle becomes energetically favorable, resulting in a hollow core. Fourth, shell thickness deceases while hollow core radius increases with additional exchange. Surface rearrangement occurs such that Ag remains the dominant surface species due to the lower surface energy of Ag vs Au[80] and facilitates additional exchange. Fifth, as the transformation continues, a bimetallic nanoparticle with locally segregated Ag and Au regions rather than a homogeneous alloy forms. Finally, transformation continues until the nanoparticle loses its structural integrity above ~65% Au.

CONCLUSION

In conclusion, we investigated the key chemical steps responsible for the transformation of citrate-capped Ag nanoparticles into AgAu nanocages in the presence of $HAuCl_4$ and sodium citrate. To this end, we used a combination of local and ensemble average characterization tools both at the nanoscale and atomic scales in order to probe the reaction as a function of $HAuCl_4$ addition. Our findings suggest that that the hollowing process cannot be explained by the nanoscale Kirkendall effect; indeed, the structural features observed during the transformation are not in line with what would be expected for Kirkendall hollowing. Rather, we find that the pathway resembles bulk Galvanic exchange, but with key differences; namely, the formation of a hollow void and the deviation from a 3:1 exchange ratio of Ag:Au, a consequence of citrate in addition to Ag playing a role in the reduction process. The atomic scale structural details elucidated in this study may also provide insight into how these particles can be used in applications where such structure is critically linked to activity, including catalysis[81] and drug delivery.[8]

ASSOCIATED CONTENT

Supporting Information

The Supporting Information is available free of charge on the ACS Publications website at DOI: 10.1021/jacs.7b06724.

Extended methods, calculation details, SAXS and EXAFS models as well as supplementary data (PDF)

AUTHOR INFORMATION

Corresponding Authors

*chadnano@northwestern.edu

*bedzyk@northwestern.edu

ORCID

Chad A. Mirkin: 0000-0002-6634-7627

Michael J. Bedzyk: 0000-0002-1026-4558

Notes

The authors declare no competing financial interest.

ACKNOWLEDGMENTS

C.A.S., S.K., C.A.M., and M.J.B. acknowledge support by the AFOSR under Award FA9550-11-1-0275. C.A.M. and L.M.M. acknowledge support from the Vannevar Bush Faculty Fellowship program sponsored by the Basic Research Office of the Assistant Secretary of Defense for Research and Engineering, and funded by the Office of Naval Research through grant N00014-15-1-0043. L.M.M. was also funded by a National Defense Science and Engineering Graduate (NDSEG) fellowship. S.K. was partially funded by DOE-BES (DE-FG02-08ER46539). M.M.S. acknowledges the SINGA fellowship by Singapore Agency for Science, Technology and Research (A*STAR) and a Postdoctoral Fellowship supported by the School of Materials Science and Engineering, Nanyang Technological University. This work made use of the EPIC facility of Northwestern University's NU*ANCE* Center, which has received support from the Soft and Hybrid Nanotechnology Experimental (SHyNE) Resource (NSF ECCS-1542205); the MRSEC program (NSF DMR-1121262) at the Materials Research Center; the International Institute for Nanotechnology (IIN); the Keck Foundation; and the State of Illinois, through the IIN. Metal analysis was performed at the Northwestern University Quantitative Bioelement Imaging Center (QBIC) supported by NASA Ames Research Center NNA06CB93G. SAXS experiments were performed at the APS DND-CAT 5ID-D beamline, which is supported through E. I. duPont de Nemours & Co., Northwestern University (NU), The Dow Chemical Co., and the NSF funded MRSEC at NU. EXAFS and XRF experiments were performed at the APS 10BM-B beamline (MR-CAT), which is supported by the Department of Energy and the MRCAT member institutions. Use of the APS was supported by DOE-BES (DE-AC02-06CH11357). We thank Steven Weigand of DND-CAT for assistance with the SAXS setup and data reduction, Joshua Wright of MR-CAT for assistance with the EXAFS setup and Keith MacRenaris of QBIC for assistance with ICP-MS.

REFERENCES

(1) Sun, Y.; Xia, Y. *Science* **2002**, *298*, 2176−2179.

(2) Pérez-Juste, J.; Pastoriza-Santos, I.; Liz-Marzán, L. M.; Mulvaney, P. *Coord. Chem. Rev.* **2005**, *249*, 1870−1901.

(3) Mohl, M.; Kumar, A.; Reddy, A. L. M.; Kukovecz, A.; Konya, Z.; Kiricsi, I.; Vajtai, R.; Ajayan, P. M. *J. Phys. Chem. C* **2010**, *114*, 389−393.

(4) Moon, G. D.; Choi, S.-W.; Cai, X.; Li, W.; Cho, E. C.; Jeong, U.; Wang, L. V.; Xia, Y. *J. Am. Chem. Soc.* **2011**, *133*, 4762−4765.

(5) Yavuz, M. S.; Yiyun, C.; Jingyi, C.; Cobley, C. M.; Qiang, Z.; Rycenga, M.; Jingwei, X.; Chulhong, K.; Song, K. H.; Schwartz, A. G.; Wang, L. V.; Xia, Y. *Nat. Mater.* **2009**, *8*, 935−939.

(6) Cho, E. C.; Kim, C.; Zhou, F.; Cobley, C. M.; Song, K. H.; Chen, J.; Li, Z.-Y.; Wang, L. V.; Xia, Y. *J. Phys. Chem. C* **2009**, *113*, 9023−9028.

(7) Ma, Y.; Li, W.; Cho, E. C.; Li, Z.; Yu, T.; Zeng, J.; Xie, Z.; Xia, Y. *ACS Nano* **2010**, *4*, 6725−6734.

(8) Skrabalak, S. E.; Chen, J.; Au, L.; Lu, X.; Li, X.; Xia, Y. *Adv. Mater.* **2007**, *19*, 3177−3184.

(9) Toshima, N.; Yonezawa, T. *New J. Chem.* **1998**, *22*, 1179−1201.

(10) Lim, B.; Jiang, M.; Camargo, P. H. C.; Cho, E. C.; Tao, J.; Lu, X.; Zhu, Y.; Xia, Y. *Science* **2009**, *324*, 1302−1305.

(11) Wang, D.; Li, Y. *Adv. Mater.* **2011**, *23*, 1044−1060.

DOI: 10.1021/jacs.7b06724
J. Am. Chem. Soc. 2017, 139, 12291−12298

(12) DeSantis, C. J.; Weiner, R. G.; Radmilovic, A.; Bower, M. M.; Skrabalak, S. E. *J. Phys. Chem. Lett.* **2013**, *4*, 3072−3082.
(13) Chen, J.; McLellan, J. M.; Siekkinen, A.; Xiong, Y.; Li, Z.-Y.; Xia, Y. *J. Am. Chem. Soc.* **2006**, *128*, 14776−14777.
(14) Skrabalak, S. E.; Au, L.; Li, X.; Xia, Y. *Nat. Protoc.* **2007**, *2*, 2182−90.
(15) Oh, M. H.; Yu, T.; Yu, S.-H.; Lim, B.; Ko, K.-T.; Willinger, M.-G.; Seo, D.-H.; Kim, B. H.; Cho, M. G.; Park, J.-H.; Kang, K.; Sung, Y.-E.; Pinna, N.; Hyeon, T. *Science* **2013**, *340*, 964−968.
(16) Niu, K.-Y.; Kulinich, S. A.; Yang, J.; Zhu, A. L.; Du, X.-W. *Chem. - Eur. J.* **2012**, *18*, 4234−4241.
(17) Sun, Y.; Xia, Y. *Anal. Chem.* **2002**, *74*, 5297−5305.
(18) Rosi, N. L.; Mirkin, C. A. *Chem. Rev.* **2005**, *105*, 1547−1562.
(19) Au, L.; Zheng, D.; Zhou, F.; Li, Z.-Y.; Li, X.; Xia, Y. *ACS Nano* **2008**, *2*, 1645−1652.
(20) Mahmoud, M. A.; El-Sayed, M. A. *J. Am. Chem. Soc.* **2010**, *132*, 12704−12710.
(21) Novo, C.; Funston, A. M.; Mulvaney, P. *Nat. Nanotechnol.* **2008**, *3*, 598−602.
(22) Xu, W.; Kong, J. S.; Yeh, Y.-T. E.; Chen, P. *Nat. Mater.* **2008**, *7*, 992−996.
(23) Wittstock, A.; Zielasek, V.; Biener, J.; Friend, C. M.; Baumer, M. *Science* **2010**, *327*, 319−22.
(24) Calver, C. F.; Dash, P.; Scott, R. W. J. *ChemCatChem* **2011**, *3*, 695−697.
(25) Song, G. L.; Atrens, A. *Adv. Eng. Mater.* **1999**, *1*, 11−33.
(26) Gonzalez, E.; Arbiol, J.; Puntes, V. F. *Science* **2011**, *334*, 1377−1380.
(27) Bi, Y.; Hu, H.; Lu, G. *Chem. Commun.* **2010**, *46*, 598−600.
(28) Sun, Y.; Mayers, B.; Xia, Y. *Adv. Mater.* **2003**, *15*, 641−646.
(29) Zhang, Y.; Sun, S.; Zhang, X.; Tang, L.; Song, X.; Yang, Z. *Phys. Chem. Chem. Phys.* **2014**, *16*, 18918−25.
(30) Métraux, G. S.; Cao, Y. C.; Jin, R.; Mirkin, C. A. *Nano Lett.* **2003**, *3*, 519−522.
(31) Personick, M. L.; Langille, M. R.; Wu, J.; Mirkin, C. A. *J. Am. Chem. Soc.* **2013**, *135*, 3800−3803.
(32) Jang, H.; Min, D.-H. *ACS Nano* **2015**, *9*, 2696−2703.
(33) Bi, Y.; Ye, J. *Chem. Commun.* **2010**, *46*, 1532−4.
(34) Chen, J.; Wiley, B.; McLellan, J.; Xiong, Y.; Li, Z.-Y.; Xia, Y. *Nano Lett.* **2005**, *5*, 2058−2062.
(35) Jiang, Z.; Zhang, Q.; Zong, C.; Liu, B.-J.; Ren, B.; Xie, Z.; Zheng, L. *J. Mater. Chem.* **2012**, *22*, 18192−18197.
(36) Xu, C.; Liu, Y.; Wang, J.; Geng, H.; Qiu, H. *ACS Appl. Mater. Interfaces* **2011**, *3*, 4626−4632.
(37) Sarkar, A.; Manthiram, A. *J. Phys. Chem. C* **2010**, *114*, 4725−4732.
(38) Schwartzberg, A. M.; Olson, T. Y.; Talley, C. E.; Zhang, J. Z. *J. Phys. Chem. B* **2006**, *110*, 19935−19944.
(39) Stamenkovic, V. R.; Mun, B. S.; Arenz, M.; Mayrhofer, K. J. J.; Lucas, C. A.; Wang, G.; Ross, P. N.; Markovic, N. M. *Nat. Mater.* **2007**, *6*, 241−247.
(40) Erlebacher, J.; Aziz, M. J.; Karma, A.; Dimitrov, N.; Sieradzki, K. *Nature* **2001**, *410*, 450.
(41) Kim, M. H.; Lu, X.; Wiley, B.; Lee, E. P.; Xia, Y. *J. Phys. Chem. C* **2008**, *112*, 7872−7876.
(42) Sun, Y.; Xia, Y. *J. Am. Chem. Soc.* **2004**, *126*, 3892−3901.
(43) Cobley, C. M.; Xia, Y. *Mater. Sci. Eng., R* **2010**, *70*, 44−62.
(44) Yin, Y.; Erdonmez, C.; Aloni, S.; Alivisatos, A. P. *J. Am. Chem. Soc.* **2006**, *128*, 12671−12673.
(45) Choi, Y.; Hong, S.; Liu, L.; Kim, S. K.; Park, S. *Langmuir* **2012**, *28*, 6670−6676.
(46) Smigelskas, A. D. K. O. *Trans. AIME* **1947**, *171*, 130.
(47) Au, L.; Lu, X.; Xia, Y. *Adv. Mater.* **2008**, *20*, 2517−2522.
(48) Fan, H. J.; Gösele, U.; Zacharias, M. *Small* **2007**, *3*, 1660−1671.
(49) Yin, Y.; Rioux, R. M.; Erdonmez, C. K.; Hughes, S.; Somorjai, G. A.; Alivisatos, A. P. *Science* **2004**, *304*, 711.
(50) Ha, D.-H.; Moreau, L. M.; Bealing, C. R.; Zhang, H.; Hennig, R. G.; Robinson, R. D. *J. Mater. Chem.* **2011**, *21*, 11498−11510.
(51) Ha, D.-H.; Moreau, L. M.; Honrao, S.; Hennig, R. G.; Robinson, R. D. *J. Phys. Chem. C* **2013**, *117*, 14303−14312.
(52) Anderson, B. D.; Tracy, J. B. *Nanoscale* **2014**, *6*, 12195−12216.
(53) Xia, X.; Xia, Y. *Front. Phys.* **2014**, *9*, 378−384.
(54) Snyder, J.; Livi, K.; Erlebacher, J. *J. Electrochem. Soc.* **2008**, *155*, C464−C473.
(55) Goris, B.; Polavarapu, L.; Bals, S.; Van Tendeloo, G.; Liz-Marzan, L. M. *Nano Lett.* **2014**, *14*, 3220−6.
(56) Smith, J. G.; Yang, Q.; Jain, P. K. *Angew. Chem., Int. Ed.* **2014**, *53*, 2867−2872.
(57) Li, H.; Xia, H.; Wang, D.; Tao, X. *Langmuir* **2013**, *29*, 5074−5079.
(58) Pinkhasova, P.; Yang, L.; Zhang, Y.; Sukhishvili, S.; Du, H. *Langmuir* **2012**, *28*, 2529−2535.
(59) Petri, M. V.; Ando, R. A.; Camargo, P. H. C. *Chem. Phys. Lett.* **2012**, *531*, 188−192.
(60) Prevo, B. G.; Esakoff, S. A.; Mikhailovsky, A.; Zasadzinski, J. A. *Small* **2008**, *4*, 1183−1195.
(61) Polte, J.; Ahner, T. T.; Delissen, F.; Sokolov, S.; Emmerling, F.; Thünemann, A. F.; Kraehnert, R. *J. Am. Chem. Soc.* **2010**, *132*, 1296−1301.
(62) Knecht, M. R.; Weir, M. G.; Frenkel, A. I.; Crooks, R. M. *Chem. Mater.* **2008**, *20*, 1019−1028.
(63) Shibata, T.; Bunker, B. A.; Zhang, Z.; Meisel, D.; Vardeman, C. F.; Gezelter, J. D. *J. Am. Chem. Soc.* **2002**, *124*, 11989−11996.
(64) Mikhlin, Y.; Karacharov, A.; Likhatski, M.; Podlipskaya, T.; Zubavichus, Y.; Veligzhanin, A.; Zaikovski, V. *J. Colloid Interface Sci.* **2011**, *362*, 330−336.
(65) Skrabalak, S. E.; Au, L.; Li, X.; Xia, Y. *Nat. Protoc.* **2007**, *2*, 2182−2190.
(66) Guinier, A.; Fournet, G. *Small-Angle Scattering of X-rays*; John Wiley and Sons: New York, 1955.
(67) Als-Nielsen, J. M. D. *Elements of Modern X-ray Physics*, 2nd ed.; John Wiley: Chichester, U.K., 2011.
(68) Ravel, B.; Newville, M. *J. Synchrotron Radiat.* **2005**, *12*, 537−541.
(69) Stern, E. A. *Contemp. Phys.* **1978**, *19*, 289−310.
(70) Stern, E. A. *Phys. Rev. B* **1974**, *10*, 3027−37.
(71) Ravel, B.; Kelly, S. D. *AIP Conf. Proc.* **2006**, *882*, 150−152.
(72) Scott, R. *Physical Methods in Bioinorganic Chemistry: Spectroscopy and Magnetism*; University Science Books, 2000.
(73) Lu, X.; Tuan, H.-Y.; Chen, J.; Li, Z.-Y.; Korgel, B. A.; Xia, Y. *J. Am. Chem. Soc.* **2007**, *129*, 1733−1742.
(74) Calvin, S.; Miller, M. M.; Goswami, R.; Cheng, S.-F.; Mulvaney, S. P.; Whitman, L. J.; Harris, V. G. *J. Appl. Phys.* **2003**, *94*, 778−783.
(75) Xia, H.; Bai, S.; Hartmann, J.; Wang, D. *Langmuir* **2010**, *26*, 3585−3589.
(76) Murshid, N.; Gourevich, I.; Coombs, N.; Kitaev, V. *Chem. Commun.* **2013**, *49*, 11355−11357.
(77) Jang, G. G.; Hawkridge, M. E.; Roper, D. K. *J. Mater. Chem.* **2012**, *22*, 21942−21953.
(78) Yang, Y.; Liu, J.; Fu, Z.-W.; Qin, D. *J. Am. Chem. Soc.* **2014**, *136*, 8153−8156.
(79) Polavarapu, L.; Zanaga, D.; Altantzis, T.; Rodal-Cedeira, S.; Pastoriza-Santos, I.; Pérez-Juste, J.; Bals, S.; Liz-Marzán, L. M. *J. Am. Chem. Soc.* **2016**, *138*, 11453−11456.
(80) Tyson, W. R.; Miller, W. A. *Surf. Sci.* **1977**, *62*, 267−276.
(81) Wang, A.-Q.; Liu, J.-H.; Lin, S. D.; Lin, T.-S.; Mou, C.-Y. *J. Catal.* **2005**, *233*, 186−197.

DOI: 10.1021/jacs.7b06724
J. Am. Chem. Soc. 2017, 139, 12291−12298